Coastal Engineering, 21 (1993) 41–69
Elsevier Science Publishers B.V., Amsterdam

Wave–current interaction within and outside the bottom boundary layer

R.L. Soulsby[a], L. Hamm[b], G. Klopman[c], D. Myrhaug[d], R.R. Simons[e] and G.P. Thomas[f]

[a]*HR Wallingford, Howbery Park, Wallingford, Oxon OX10 8BA, UK*
[b]*SOGREAH Ingénierie, BP 172, 38042 Grenoble Cedex, France*
[c]*Delft Hydraulics, P.O. Box 152, 8300 AD Emmeloord, Netherlands*
[d]*Division of Marine Hydrodynamics, Norwegian Institute of Technology, N-7034 Trondheim-NTH, Norway*
[e]*Civil and Environmental Engineering, University College London, Gower Street, London WC1E 6BT, UK*
[f]*Dept. of Mathematical Physics, University College, Cork, Ireland*

(Received 1 October 1992; accepted after revision 1 June 1993)

ABSTRACT

This paper reviews the state-of-the-art as perceived by the Wave–Current Interaction (WCI) group which forms part of the MAST G6M Coastal Morphodynamics project, and includes some new results arising out of that project. Those processes which affect the vertical profiles of current and wave kinematics, and the bed shear-stresses, are discussed, but "horizontal" processes such as refraction of waves by currents, and generation of longshore currents, are not included. Among the group's conclusions are recommendations for the calculation of wave-induced bottom orbital velocities with and without WCI, and direct parameterisations of the bed shear-stresses produced by WCI. The latter is the result of a comprehensive intercomparison of WCI boundary-layer models and data. The results are aimed at aiding the formulation of numerical models of coastal morphodynamics.

INTRODUCTION

The hydrodynamics of the coastal zone is dominated by two equally important factors: waves and currents. The waves are usually generated by the wind, while the currents may be driven by the tides, the wind, the waves, density variations or river outflows. Their combined effect has many engineering applications, but of special interest in this paper is the movement of sediment on the sea-bed, and the consequent evolution of the coastal morphology.

The wave and current fields interact mutually through a number of mechanisms:

(a) refraction of the waves by horizontally sheared currents
(b) modification of the wave kinematics by the (possibly vertically sheared) current

(c) generation by the waves of "mass transport" or "streaming" currents
(d) generation by the waves of radiation stresses giving rise to currents, particularly longshore currents in the surf zone
(e) enhancement of the bottom friction felt by the currents, due to interaction with the wave boundary layer
(f) enhancement of the bed shear-stresses and energy dissipation of the waves, due to interaction with the current boundary layer.

We are only concerned in this paper with wave–current interaction (WCI) in the vertical plane, and so we will concentrate only on mechanisms (b), (c), (e) and (f). In particular, we wish to focus on those aspects of these mechanisms which are most relevant to sediment transport and coastal morphodynamic modelling. For this, we need to predict the geographical distributions of the waves and currents, the vertical profile of the currents, the wave-induced orbital velocity near the bed, and the time-varying bed shear-stresses.

Although the surf-zone is one of the areas of most intense sediment transport, most of the theoretical effort in wave–current interaction has been restricted to nonbreaking waves, for simplicity, and this restriction applies also in this paper. Nonetheless, the theories are often applied (with an unknown degree of error) to surf-zone conditions also. Recent experiments by Deigaard et al. (1991) showed that the bed shear-stresses in the surf zone were not *on average* very different from those offshore of the breaker point, but they exhibited much greater wave-to-wave variability, so that occasional very large values could occur.

Major reviews, which also deal with mechanisms (a) and (d), have been presented by Peregrine (1976), Grant and Madsen (1986), Jonsson (1990), and Sleath (1990b).

WAVE–CURRENT INTERACTION THROUGH THE WATER COLUMN

Wave kinematics without currents

Before moving to the case of combined waves and currents, it is useful to review the prediction of wave kinematics with no mean current superimposed. Wave kinematics prediction is a task involved in a large number of engineering problems covering two main fields, (a) the design of offshore and nearshore structures, and (b) the computation of sediment transport on the shoreface and in the nearshore zone.

To achieve this task, many wave theories are available, but they can lead to quite different results. A short review of the most widely used models is available in a companion paper in this issue (Hamm et al., 1993).

Historically, many comparison studies have focused on the prediction of the horizontal velocity under the crest, which is one of the most important quantities used for design purposes (Dean and Perlin, 1986; Kirkgöz, 1986).

The main result of interest for sediment transport computations is that, *near the bottom*, the linear theory gives the best overall agreement with data for flat and sloping beds (slopes between 1:100 and 1:4.45) up to the breaking point and within the surf-zone. Eq. (1) gives an explicit version of the linear horizontal velocity which is accurate within 1% for $k_0h<1.54$ (Nielsen, 1984)

$$u_{bc}=0.5H(g/h)^{0.5}(1-k_0h/3) \tag{1}$$

where u_{bc} is the orbital velocity near the bed under the wave crest, H is wave height, g is acceleration due to gravity, h is water depth, and k_0 is the deep-water wavenumber.

It should be pointed out that this very flattering comparison cannot be extrapolated to the overall velocity profile (Hattori, 1986). In particular, velocities under the trough are overestimated by a factor reaching 1.5 to 2 near the breaking point due to asymmetries. The asymmetry can be very important in determining the direction and magnitude of the net sediment transport by the waves. This is often computed from velocity moments (i.e. the mean over a wave cycle of powers of the orbital velocity or its modulus). Nadaoka and Kondoh (1982) presented curves of skewness of near-bottom horizontal velocity of shoaling waves (Fig. 1). They show that asymmetries reach a maximum near the breaking point and then decrease in the surf zone except for waves with a high offshore steepness (spilling breakers).

This weakness in predicting velocity asymmetries could be overcome by Stokes higher order models in intermediate depths, when vertical asymme-

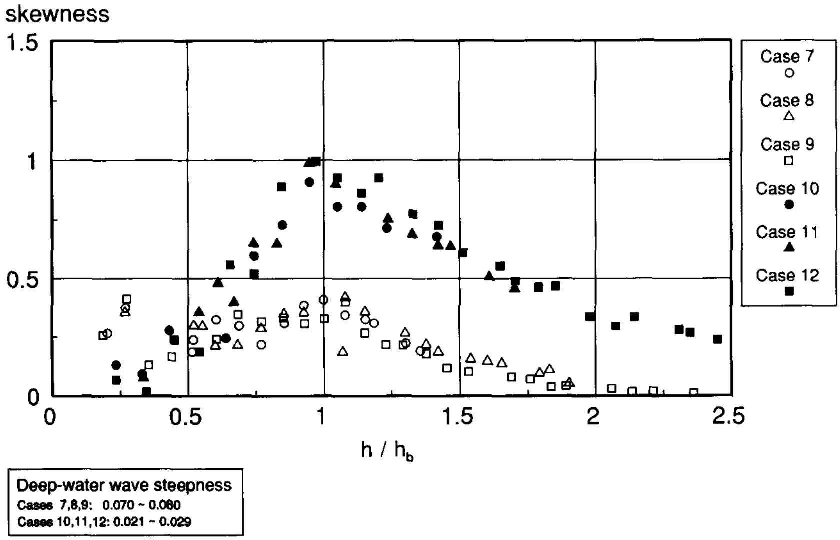

Fig. 1. Distribution of velocity skewness of shoaling waves on a 1:20 plane beach before and after the breaking point (h_b). From Nadaoka and Kondoh (1982).

tries are weak, but not in the nearshore zone. In that case, several semi-empirical methods are proposed in the literature.

Biesel (1951) was among the first to derive a wave theory on a sloping bottom based on a Stokes perturbation approach. Comparisons with measured asymmetry parameters related to shoaling wave profiles and associated near-bottom velocities have been reported by Adeyemo (1968, 1970) with reasonable agreement. Subsequently, Svendsen and Buhr-Hansen (1977) followed the same philosophy to extend the classical cnoidal theory to shoaling waves. They focused on the prediction of wave profiles and reported very good agreement with measured data for Ursell numbers up to 500.

From harmonic analysis of regular shoaling wave profiles, Flick et al. (1981) have shown that classical wave theories derived on a flat bottom can adequately predict amplitudes of the harmonics, but not phase lags which are locked to zero in the models. Following that idea, Hattori and Katsurakawa (1990) have proposed empirical formulae of phase lags to improve velocity predictions, but did not check them against measured near-breaking velocity measurements. This method could be implemented in models based on Fourier developments.

Isobe and Horikawa (1982) have proposed empirical corrections of the linear theory. In this model, the bottom velocity under the wave trough u_{bt} is expressed as:

$$u_{bt} = -u_{bc}(1 - r_2 exp(-r_3(h/\lambda_0))) \tag{2}$$

with

$$r_2 = 3.2(H_0/\lambda_0)^{0.65} \quad \text{and} \quad r_3 = -27 log(H_0/\lambda_0) - 17$$

where H_0 is the deep-water wave-height, and $\lambda_0 = 2\pi/k_0$ is the deep-water wavelength. This method has not been checked against another independent data-set.

Finally, Swart and Crowley (1988) published a parameterisation of results obtained with a new numerical theory (called the covocoidal theory) which solves the Laplace equation with the associated boundary conditions on a sloping bottom. This method is claimed to be very versatile, including the Stokes and cnoidal domains up to the breaking point. Comparisons against laboratory data of Isobe and Horikawa (1982) are presented in Fig. 2. In these cases, this method improves significantly the prediction of orbital velocities and velocity moments. However, more verification is needed in order to assess the accuracy of the method itself and of its parameterisation.

When randomness of waves is considered, the situation becomes complicated by the presence of bound and free low frequency waves. Roelvink and Stive (1989) have presented good comparisons between computed and measured velocity moments in a flume. A comprehensive approach is still not available at the moment.

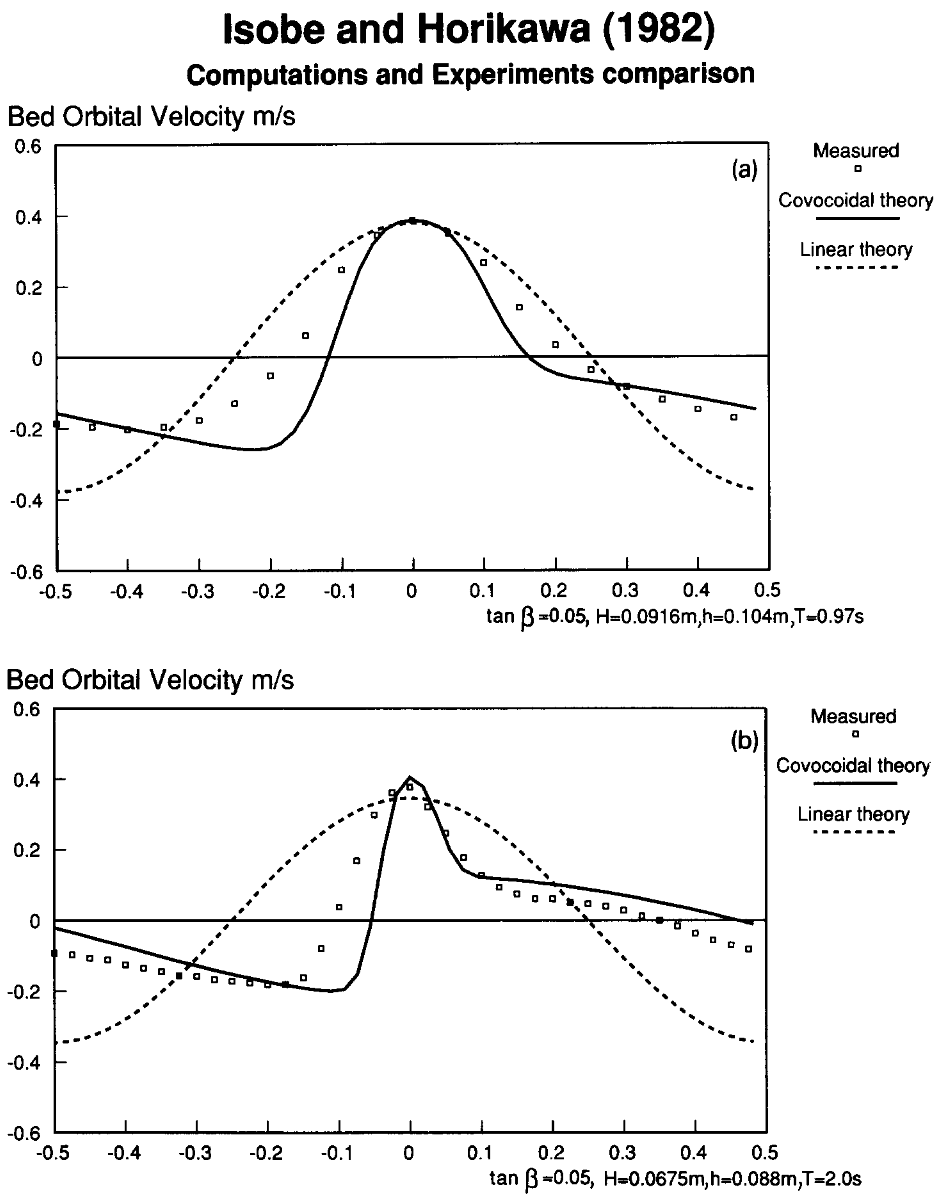

Fig. 2. (a,b) Comparison of computed and measured velocity profiles of shoaling waves on a 1:20 plane beach.

Wave kinematics with shear currents

We next examine the effect on the wave kinematics of adding a current to the wave. The vertical variation in the current profile can be of crucial importance in the wave–current interaction process. If the vorticity distribution is globally important, then models which take full account of the vorticity distribution should generally be used. If the vorticity is important only in a restricted area of the profile, as is the case when there is a narrow shear layer, then vorticity models must be used if accurate results are required near the shear layer; elsewhere in the flow, irrotational wave models, corresponding to currents with constant vorticity, can often be used to good effect. However, even for currents with a global distribution of vorticity, it is still possible to find simple approximations which work well in certain areas of the flow field.

To illustrate these concepts a commonly occurring current profile is used to consider interactions in both the linear and nonlinear wave regimes: this is the generic tidal current profile proposed by Soulsby (1990),

$$\begin{aligned} U(z) &= 1.104(1+z/h)^{1/7}U_{\max} \qquad -1 \leqslant z/h \leqslant -0.5 \\ &= U_{\max} \qquad\qquad\qquad\qquad\quad -0.5 \leqslant z/h \end{aligned} \tag{3}$$

where $U(z)$ is the current speed at depth $(-z)$, and $U_{\max}$ is the current speed at the surface. A useful quantity associated with this profile is U_{mean}, defined to be the constant current with the same mass flux as $U(z)$ when the domain of $U(z)$ extends to the mean free surface, $z=0$. Consequently U_{mean} is a constant multiple of $U_{\max}$ and the constant of proportionality is 0.937.

One important feature of the profile in Eq. (3) is the extremely strong shear layer in the immediate vicinity of the bed. This shear does not appear in Soulsby's collation of data, nor is zero bed velocity necessary in an inviscid, low turbulence model. To prevent numerical instabilities, this strong bottom shear is removed and approximated by a more amenable form; this is shown as the mean profile in Fig. 3. Such an approximation is readily justified in terms of the present model describing the external flow to a boundary layer close to the bed.

The current distribution Eq. (3), with the amendment outlined above, is employed with the following data set to investigate the influence of the global shear, which is clearly strongest in the vicinity of the bed,

$$h = 10\ \mathrm{m}, \quad T = 10\ \mathrm{s}, \quad U_{\max} = \pm 1\ \mathrm{ms}^{-1} \tag{4}$$

To gain an understanding of the importance of the shear, the wavelength λ and velocity profiles are calculated using exact and approximate methods in the linear and nonlinear regimes. Particular attention is directed to the horizontal orbital velocity, u_{bc} and u_{bt}, evaluated at the bed under wave crest and trough respectively; in the linear regime these two quantities are equal and can be written as u_{b}. Analytical solutions do not exist for current profiles which contain arbitrary distributions of vorticity in either the linear or nonlinear regimes and numerical methods must be used.

For linear waves the interaction is governed by the Rayleigh equation. Solutions are not difficult to obtain and the method used here is the one de-

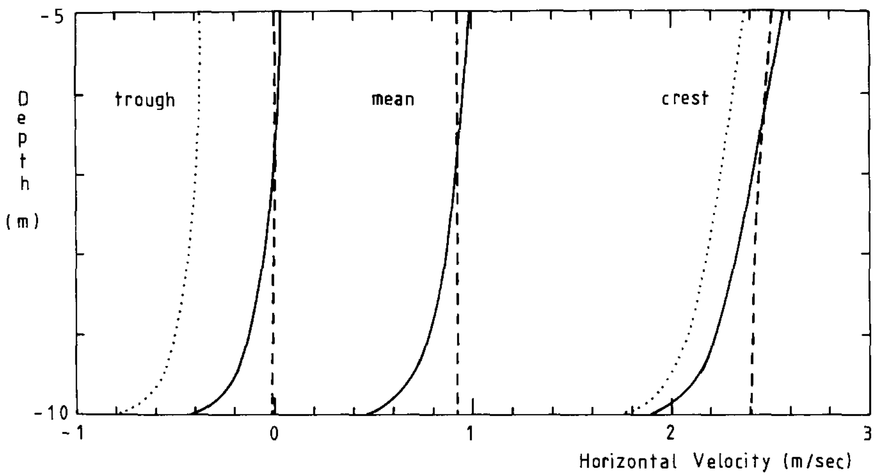

Fig. 3. Horizontal velocity profiles under the wave crest and trough for the region within 5 m of the bed; the appropriate current profiles are also shown. (——) Exact rotational theory, (– – –) approximate irrotational theory, (·····) linear theory.

scribed by Thomas (1981). More recently, approximate methods using a "weak current" approach have been used to seek semi-analytic solutions in the linear regime. In this case the representative current speed is assumed to be small relative to the phase speed of the waves. Attention has primarily been directed towards the dispersion relation and the extension of this approach to finite depth was given by Kirby and Chen (1989). This "weak current" approximation is often valid and deserves attention.

The predictions from three models are compared for the linear wave regime, with a wave amplitude of 0.25 m. The first is the exact Rayleigh equation, the second is the first order weak current approximation of Kirby and Chen (denoted by "K&C") and the third is the irrotational model for a depth constant current U_{mean}. The kinematic expressions for the velocity field derived by Kirby and Chen do not take proper account of the surface boundary condition, although their dispersion relationships are valid; the correct form is used here.

The wavelength predictions presented in Table 1 are in good agreement for all three models with both following and adverse currents; relative to the exact Rayleigh equation the wavelength errors are of the order of 0.1%. The complete velocity profile predictions, not presented here, were found to possess approximately the same magnitude of errors for both following and adverse currents. For K&C, the maximum error of 0.2% in the horizontal orbital velocity component occurs at the bed, and the RMS error over the whole depth is 0.05%. For the constant current U_{mean} the maximum error also oc-

TABLE 1

Wavelength and bottom orbital velocity predictions from Exact rotational, approximate rotational (KandC) and approximate irrotational (U_{mean}) linear wave models

	$U_{max}=1$ m/sec		$U_{max}=-1$ m/sec	
	λ	u_b	λ	u_b
Exact	103.07	0.2103	81.17	0.2156
K&C	103.06	0.2099	81.16	0.2151
U_{mean}	102.93	0.2199	81.38	0.2058

TABLE 2

Wavelength and bottom orbital velocity predictions from Exact rotational and approximate irrotational (U_{mean}) finite amplitude wave models

	$U_{max}=1$ m/sec			$U_{max}=-1$ m/sec		
	λ	u_{bc}	u_{bt}	λ	u_{bc}	u_{bt}
Exact	106.93	1.416	0.888	84.30	1.377	1.042
U_{mean}	106.61	1.477	0.934	84.69	1.320	0.992

curs at the bed and the corresponding error values are 4.5% and 1.5% respectively.

For finite amplitude waves exact solutions are obtained numerically using the method presented by Thomas (1990), which is based upon the original work of Dalrymple (1973). Irrotational wave motions, corresponding to the constant current U_{mean}, are modelled by finite amplitude fifth order Stokes' waves. The wave height H was given a value of 3 m. For these nonlinear wave theories h is taken to be the mean water depth and $U(z)$ is only defined below the wave trough.

Detailed velocity profiles under the wave crest and trough for the region within 5 m of the bottom for $U_{max}=1$ m s^{-1} are shown in Fig. 3; the corresponding curves for $U_{max}=-1$ m s^{-1} demonstrate essentially the same quantitative features and are not included. The wavelength and bottom orbital velocity predictions for this finite amplitude wave–current interaction are given in Table 2.

The solid curves in Fig. 3 correspond to the exact solution, obtained using seven harmonics to define the free surface; the broken lines correspond to the Stokes fifth order theory for U_{mean} and the dotted lines represent the exact linear theory for the rotational current $U(z)$. It is clear from the figure that if accurate estimates of the velocities are required, then it is important to include the influence of both the vorticity and finite amplitude effects.

The wavelength predictions presented in Table 2 are not strongly dependent upon the vorticity and good estimates are obtained using the approximate irrotational finite amplitude wave model. It is not sufficient to use a linear model which takes account of the current vorticity, as can be seen by comparing the wavelength predictions in Tables 1 and 2.

The orbital velocities u_{bc} and u_{bt} at the bed are also shown in Table 2. These are measured relative to the local current in each case and the values obtained using the constant current are accurate to about 6% of the exact values for both the crest and trough. This degree of agreement is somewhat surprising, given the strong necessity for exact models to predict velocity profiles, as demonstrated by Fig. 3. Linear theory predictions will not be very accurate for the bottom orbital velocity as the degree of asymmetry between crest and trough is appreciable.

To investigate this agreement between exact rotational and approximate irrotational finite amplitude wave models for bottom orbital velocities more generally, the quantities u_{bc} and u_{bt} were calculated for the same test data Eq. (4), with the wave height varied between 0 m and 4 m. The results for $U_{max} = 1$ m s^{-1} are shown in Fig. 4; as before there was insufficient quantitative difference shown by $U_{max} = -1$ m s^{-1} to necessitate inclusion. The same curve designations are used as for Fig. 3, i.e. the solid, broken and dotted lines correspond to the exact, Stokes fifth order (constant current) and exact linear models, respectively.

The figure confirms the conclusion drawn from Table 2 — good estimates can be obtained using an irrotational, constant current, finite amplitude wave

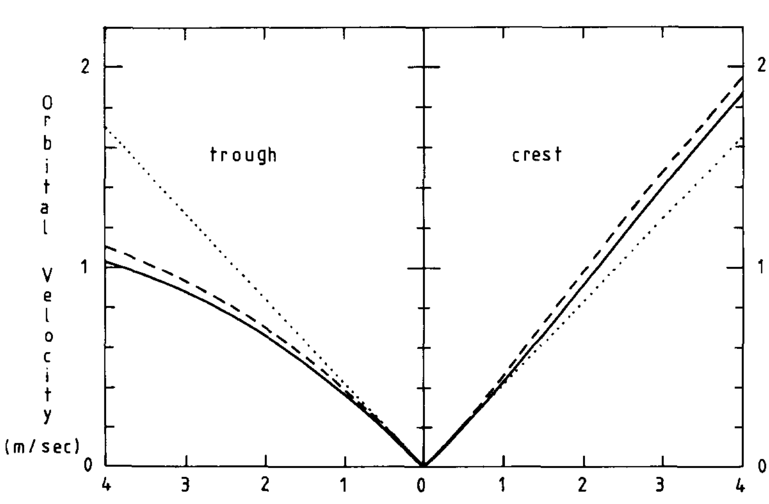

Fig. 4. The variation of bottom orbital velocity under the wave crest and trough with increasing wave height. Curve definitions as for Fig. 3.

model. The linear theory provides relatively poor estimates for the bottom orbital velocity but the presence of the linear theory curves clearly illustrates the importance of asymmetry.

Fluid-friction effects on wave kinematics and mean flow

Although the wave kinematics outside the bottom and free-surface boundary-layers can be modelled quite accurately using frictionless theories, as in the preceding section, fluid-friction effects dominate the wave-induced changes in the mean flow. For the case of water waves without a current, Longuet-Higgins (1953) studied the bottom and free-surface boundary-layers, and the influence of the waves on the mean-Lagrangian motion over the full water depth. Among others, this was extended by Craik (1982), taking surface contamination and spatial and temporal wave attenuation into account, both for a mean-Eulerian and mean-Lagrangian description of the mean flow. Numerical solutions of the mean-Lagrangian motion in water waves were presented recently by Iskandarani and Liu (1991a,b).

For the case of wave–current interaction, and a viscous flow with constant kinematic viscosity ν, the wave-part of the flow is described to first order by the Orr-Sommerfeld equation, as frequently used in the theory of hydrodynamic stability, e.g. Drazin and Reid (1981), §25:

$$\left(i\frac{k}{\nu}\right)^{-1}\left(\frac{\mathrm{d}^2}{\mathrm{d}z^2}-k^2\right)^2\tilde{w}=-\frac{\sigma_0}{k}\left(\frac{\mathrm{d}^2}{\mathrm{d}z^2}-k^2\right)\tilde{w}-\frac{\mathrm{d}^2U}{\mathrm{d}z^2}\tilde{w} \qquad (5)$$

with $\tilde{w}(z)$ the complex-valued first-order vertical-velocity amplitude, $U(z)$ the zeroth-order undisturbed mean-flow velocity, $\sigma_0(z)=\sigma-kU(z)$ the intrinsic wave frequency, k the wave number, σ the absolute wave frequency, and where a tilde denotes the wave-part of a quantity. The Orr-Sommerfeld equation describes the oscillatory part of the flow from the bottom to the free surface, including the bottom and free-surface boundary layers.

Due to friction, the waves decay either in the space- or time-direction, and thus k and/or σ are complex-valued. The horizontal-velocity amplitude $\tilde{u}$ is readily obtained from the continuity equation:

$$ik\tilde{u}+\frac{\mathrm{d}\tilde{w}}{\mathrm{d}z}=0 \qquad (6)$$

The Orr-Sommerfeld equation can only be solved analytically for simple flows, i.e. flows with constant basic shear $\mathrm{d}U/\mathrm{d}z$. In more complicated cases one has to use approximate methods or numerical solution methods, see Drazin and Reid (1981). For the case of vanishing viscosity, Eq. (5) reduces to Rayleigh's stability equation, as studied by Thomas (1981). For the core region of the fluid flow, outside the bottom and free-surface boundary layers, Rayleigh's stability equation is a good approximation.

The above formulations are all for a constant viscosity, which is appropriate for laminar flows. Klopman (1992) describes the equations for waves on a turbulent current, up to second-order in wave-slope, using a multiple-scales perturbation-series approach. A turbulence model is used for the prediction of the eddy-viscosity distribution. The resulting ordinary differential equations, describing the flow from the bed to the free surface, have to be solved numerically.

An example is given in Fig. 5 which corresponds to the flow conditions in test V20 of Bakker and Van Doorn (1978): a wave height of 0.12 m, a mean water depth of 0.3 m, a wave period of 2 s and a mean depth-averaged velocity of 0.2 m s^{-1}. Prandtl's mixing-length model was used for the description of the eddy-viscosity. A logarithmic current-profile was used as a zeroth-order (basic) solution. The first-order complex-valued amplitudes of the horizontal velocity $\tilde{u}$, vertical velocity $\tilde{w}$, dynamic pressure $\tilde{p}$ and shear stress $\tilde{\tau}_{xz}$ are plotted as a function of the vertical coordinate $(z+h)$. The real part of the solution is in phase with the first-order free-surface elevation $\tilde{\zeta}$, and the imaginary part is 90° out of phase with $\tilde{\zeta}$. Outside the bottom boundary-layer $\tilde{u}$, $\tilde{w}$ and $\tilde{p}$ are almost identical to the potential-flow linear wave-theory values. Within the bottom boundary-layer $\tilde{u}$ shows the behaviour as found from

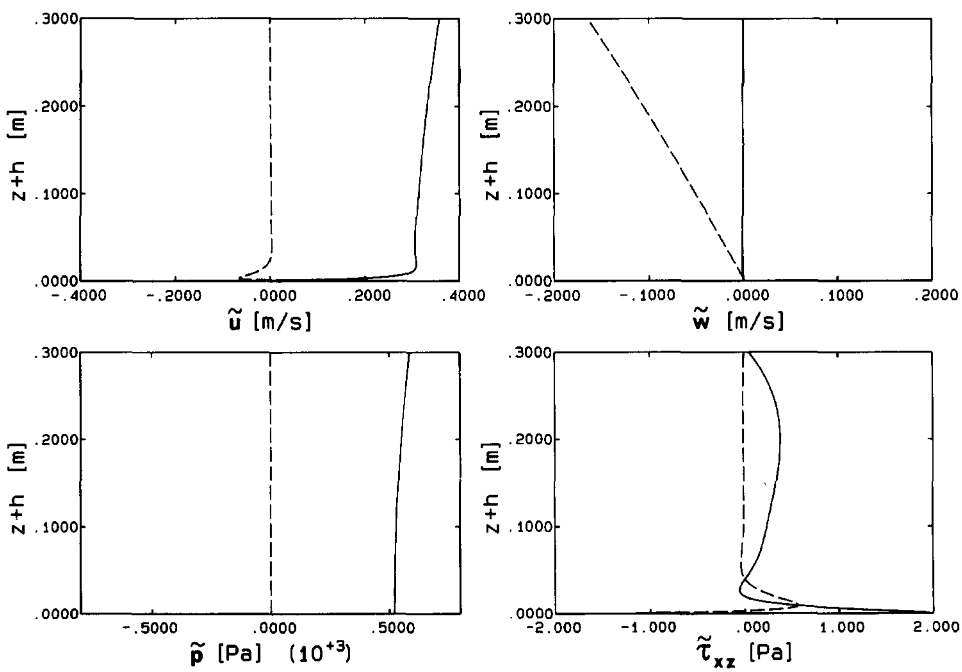

Fig. 5. First-order solution for Prandtl's mixing-length model. $\tilde{u}$, $\tilde{w}$, $\tilde{p}$ and $\tilde{\tau}_{xz}$ as a function of $(z+h)$. (——) Real part, (– – –) imaginary part.

boundary-layer models: an overshoot of $|\tilde{u}|$ at the edge of the boundary layer and large phase shifts through the boundary layer. The shear stress $\tilde{\tau}_{xz}$ does not vanish outside the bottom boundary layer, in contrast with potential flow theory where $\tilde{\tau}_{xz}$ is equal to zero.

The second-order changes in the mean horizontal velocity under combined wave–current motion are mainly due to three reasons: the mean value of Reynolds-averaged wave shear-stress $\overline{\tilde{u}\tilde{w}}$ is non-zero, in contrast with inviscid theories. Secondly, the presence of waves changes the mean shear-stress just outside the bottom and free-surface boundary-layers. Thirdly, the spatial and temporal decay of the waves induces momentum and mass transfer between different layers. This last point was studied by Craik (1982) for the case of waves without a current, and a constant viscosity.

An important question is whether one should use a mean-Eulerian or mean-Lagrangian description of the mean flow. For the description of suspended matter, such as fine sediments, it seems that a mean-Lagrangian description is more appropriate. Since the suspended sediment will move with about the same velocity as the fluid particles, the wave phase-averaged sediment motion will be related more closely to the mean-Lagrangian than to the mean-Eulerian fluid velocity. From pure wave motion we know that the mean-Eulerian and mean-Lagrangian (Stokes drift) velocity profiles are quite different, also near the bottom boundary layer. In wave–current flow, a rigorous approach is possible by using the generalized Lagrangian-mean (GLM) formulation of Andrews and McIntyre (1978a,b). Although complicated, this GLM formalism is of general applicability for deriving Lagrangian-mean equations of motion. However, no results are known for applications in turbulent wave–current flows.

Most boundary-layer models describe flows which are parallel to the bottom, and they can not describe the mean-Lagrangian motion found in water wave flows (which also have a vertical velocity component). Noteworthy exceptions are the analytical model of Trowbridge and Madsen (1984a,b) and the numerical model of Trowbridge et al. (1986).

BOTTOM FRICTION

Intercomparison of models

The boundary layers at the sea-bed associated with the waves and the current interact nonlinearly, because they are dominated by turbulent shear-stresses and turbulence generation is a nonlinear phenomenon. If shear-stresses are linearly proportional to velocities (as in laminar conditions) then the problem is trivial and the waves and currents remain independent. However, turbulent shear-stresses are proportional to the square of velocities, and hence the turbulence generated by the waves affects the currents, and vice versa.

This has the effect of enhancing both the mean and oscillatory shear-stresses (Fig. 6). In addition, the current profile is modified, because the extra turbulence generated close to the bed by the waves appears to the current as being equivalent to an enhanced bottom roughness. Many models have been put forward to describe the combined boundary layer: a list of 21 models was compiled by the G6M group in January 1991, and several new models have appeared since then. We make an intercomparison here between only those models which were either devised by, or used by, members of the G6M group. These include the analytical models with time-invariant eddy viscosity of Grant and Madsen (1979) and Christoffersen and Jonsson (1985); the analytical mixing-length models of Bijker (1967) and Van Kesteren and Bakker (1984), the momentum-defect model of Fredsøe (1984), the similarity model of Myrhaug and Slaattelid (1990), and the fully numerical models employing turbulent-energy closure of Davies et al. (1988) and Huynh-Thanh and Temperville (1991). Other models are recognized as important (e.g. Tanaka et al. 1983; O'Connor and Yoo, 1988; Sleath, 1991) but time-constraints have precluded them from this intercomparison.

For sediment transport purposes it is important to predict the time-mean bed shear-stress τ_m and the maximum bed shear-stress τ_{max}, in the combined wave–current flow (Fig. 6). The threshold of motion and entrainment of the sediment are determined by τ_{max}, while the current velocity and the diffusion of suspended sediment into the upper part of the flow are determined by τ_m. It is convenient to distinguish between the bed-shear stresses which would occur if nonlinear interaction did not take place, so that the shear-stresses generated by the wave-alone and the current-alone could be summed linearly, and the nonlinear enhancement which it is the primary purpose of the models

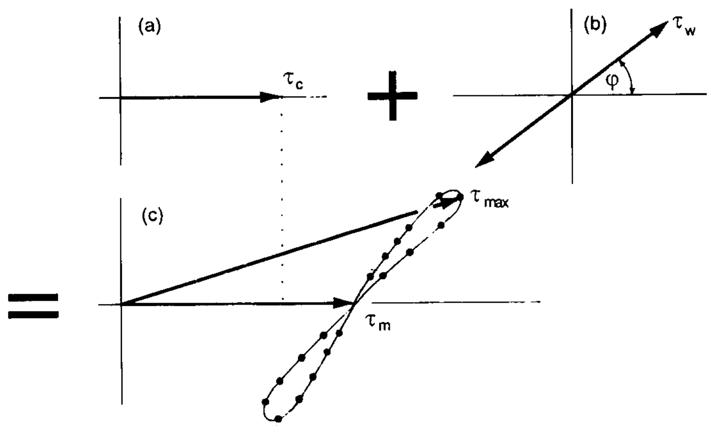

Fig. 6. Schematic of bed shear-stresses with WCI. (a) The current-alone stress (τ_c), and (b) the wave-alone stress (amplitude = τ_w), combine nonlinearly to give (c) the locus of the combined WCI stresses, having mean τ_m and maximum τ_{max}.

to predict. We have therefore presented results from all the models in terms of the nondimensional parameters $y \equiv \tau_m/(\tau_c+\tau_w)$ and $Y \equiv \tau_{max}/(\tau_c+\tau_w)$, where τ_c is the bed shear-stress produced by a current-alone having the same depth-averaged speed U_{mean} as for the combined case, and τ_w is the maximum bed shear-stress of a wave-alone having the same bottom orbital velocity amplitude u_b as for the combined case. These are plotted against $x \equiv \tau_c/(\tau_c+\tau_w)$ which is a measure of the relative strengths of the current and the wave, whose value ranges from 0 for waves-alone to 1 for current-alone conditions. The stresses τ_c and τ_w can be calculated directly from the input variables U_{mean} and u_b via the relationships $\tau_c = \rho C_D U_{mean}{}^2$ and $\tau_w = 0.5\rho f_w u_b{}^2$, where C_D is the drag coefficient for the current U_{mean} on its own, f_w is the wave friction factor for an orbital velocity u_b on its own, and ρ is water density. In the absence of nonlinear interaction we obtain $Y=1$ for co-linear waves and currents. For waves directed at an angle ϕ to the current, a linear vector addition gives $Y=[x^2+(1-x)^2+2x(1-x)\cos\phi]^{1/2}$. Since $\tau_m=\tau_c$ in the absence of nonlinear interaction, we have $y=x$ for all ϕ.

Apart from ϕ and x, the other input parameters required by the models are z_0/h and A/z_0, where z_0 is the physical bottom roughness length, and $A=u_b/\sigma$. It is assumed that the bed is immobile and hydrodynamically rough, the waves are not breaking, and the bottom orbital velocity is horizontal and sinusoidal with time.

The eight models have been run for the 24 combinations $z_0/h=10^{-5}, 10^{-4}, 10^{-3}$; $A/z_0=10^2, 10^3, 10^4, 10^5$; $\phi=0°, 90°$; and sufficient values of x to resolve the curves. Three of the models have additionally been run for $\phi=15°$, 30°, 45°, 60°, 75°. Only the 18 combinations of input parameters yielding $A/h<1.5$ are considered to be physically meaningful.

An example for the case $z_0/h=10^{-4}$, $A/z_0=10^4$, $\phi=0°$ is shown in Fig. 7. It can be seen that: (a) predictions of Y vary by up to 30%; (b) predictions of y vary by typically 35%, and by up to a factor of 4 for wave-dominated conditions; (c) the models of Grant and Madsen (1979), Christoffersen and Jonsson (1985), and Myrhaug and Slaattelid (1990) have a distinctly different behaviour from the other models for y in current dominated conditions $(0.5<x<1)$.

The intercomparisons for all 24 combinations of inputs, which will be reported fully in a later publication, show the following trends for all the models except Bijker (1967): (d) the strength of the nonlinear enhancement of both y and Y increases with increasing z_0/h and increasing A/z_0, and decreases as ϕ goes from 0° to 90°; (e) differences in y between the models increase with z_0/h and A/z_0, but differences in Y increase with z_0/h and decrease with A/z_0; (f) for $\phi=90°$, the differences between models is relatively small, and the distinct behaviour of the three models noted in (c) is not apparent. The Bijker model does not vary with z_0/h and A/z_0 when plotted in these coordinates: it

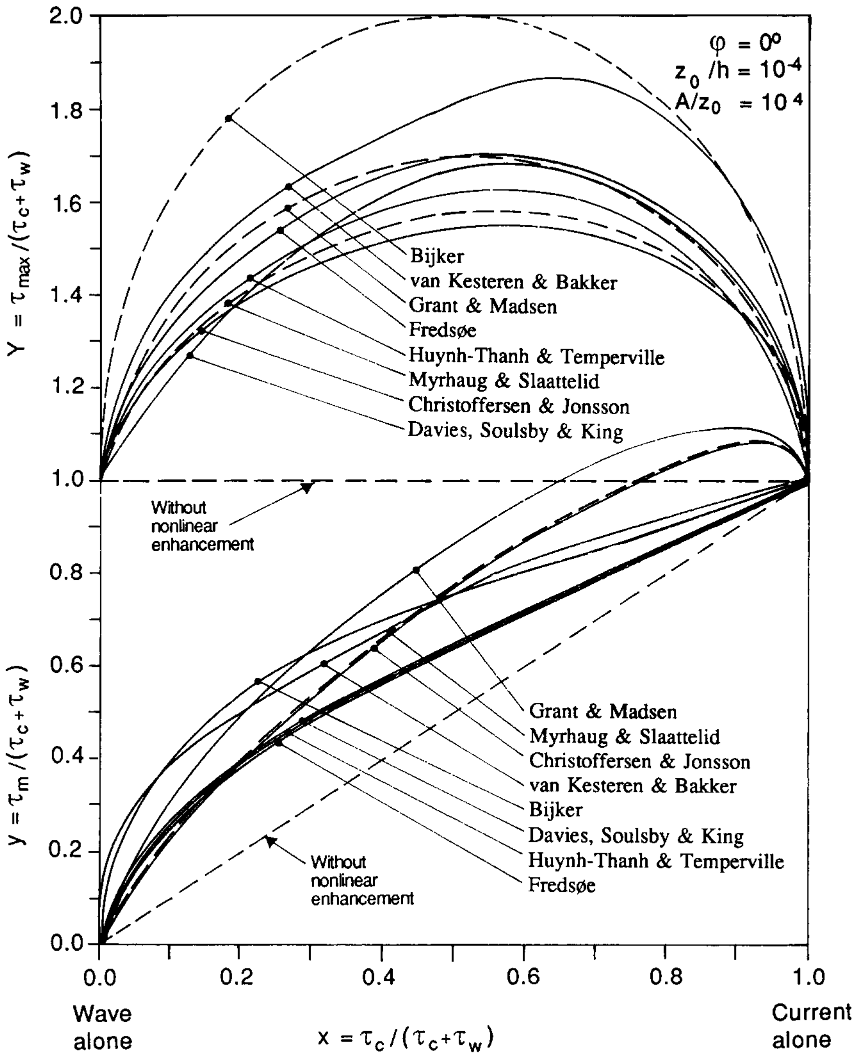

Fig. 7. Intercomparison of WCI models of Bijker (1967), Christoffersen and Jonsson (1985), Davies et al. (1988), Fredsøe (1984), Grant and Madsen (1979), Huynh-Thanh and Temperville (1991), Myrhaug and Slaattelid (1990), and Van Kesteren and Bakker (1984).

generally predicts much stronger nonlinear enhancement of y and Y than the other models.

A test by A.G. Davies (pers. commun.) in which the Davies et al. (1988) model was run first with full turbulent-energy closure, and then with time-invariant eddy-viscosity equal at each height to the maximum value from the first run, reproduced the large values of y for strong co-linear currents noted in (c) above. It would therefore appear that this behaviour results from the use of τ_{max} to scale the eddy viscosity at all phases of the wave cycle. If τ_m is used for scaling instead, the anomolous behaviour does not appear, but smaller stresses are obtained throughout. If a steady-plus-sinusoidal eddy viscosity is used, then a rather small oscillatory contribution is sufficient to suppress the anomolous behaviour.

Previous published comparisons between models, such as those by Dyer and Soulsby (1988), Simons et al. (1988), and O'Connor and Yoo (1988), showed larger differences between models than those shown in Fig. 7. This may be partly due to the fact that y and Y are nondimensionalised by $(\tau_c + \tau_w)$. Conversion to absolute values of τ_m and τ_{max} requires in addition values of C_D for a current-alone and f_w for waves-alone, both of which are found to vary significantly between the models examined here, so that this may also cause larger differences between models.

Experimental data

Reliable data against which wave–current models can be validated are in rather short supply. This is due in part to the experimental difficulties of generating appropriate conditions in the laboratory, but can also be attributed to the expense and inadequacy of instrumentation capable of making the necessary measurements of velocity and shear stress, either under laboratory or field conditions, from which shear stresses can be derived.

The experiments carried out can be grouped into three categories, namely, flume tests with co-linear waves and current, laboratory tests with orbital motion orthogonal to the current, and field experiments where waves propagate at various angles to the current. Shear stresses have been deduced from a variety of different methods, for instance, from the water surface properties, from mean and ensemble averaged "constant stress" velocity profiles, from inertial dissipation of turbulence, and from direct bed-mounted shear stress sensors.

The earliest paper providing reliable shear stress data was that by Bakker and Van Doorn (1978), who made detailed measurements with a LDV for two cases of waves on a following current over a rough bed. Kemp and Simons (1982, 1983) carried out 4 similar tests, and included 5 cases where waves propagated on an opposing current. In both cases, mean shear stresses deduced from logarithmic mean velocity profiles were found to be increased by the addition of waves, as was the apparent bottom roughness felt by the mean flow. Asano and Iwagaki (1984) reported three cases of waves on a following current over a two-dimensional bed roughness. Although LDV was used in the tests, shear stresses were deduced from mean water surface slope and wave attenuation rates. Asano et al. (1986) carried out tests with waves on an opposing current, determining shear stresses from the mean velocity profiles and observing similar increases to those of Bakker and van Doorn. Large scale tests were carried out by Myrhaug et al. (1987) over an extreme three-dimensional bed roughness using a towed carriage oscillating at 10 s period. Shear stresses, again, came from log profiles, as they did in Simons et al. (1988), who reported 24 combinations of wave and following current over a gravel bed. Further experiments in a wave–current flume at Delft Hydraulics are planned as part of the MAST G8-M programme.

Both Bijker (1967) and Visser (1986) carried out tests on waves propagating orthogonally across a turbulent current, deducing mean shear stresses from the water surface slope. Simons et al. (1992) have carried out tests in a similar wave basin as part of the present MAST G6-M programme. They used a novel shear plate set in a fixed sand-roughened bed to make direct measurements of shear stress in conjunction with a fibre-optic LDV system. Sleath (1990a) has also obtained measurements of bottom shear stress from logarithmic velocity profiles, in this case simulating the orthogonal oscillatory flow field by oscillating a section of the bed of a flume across the line of a turbulent current. 22 different flow combinations were considered in this study. Sleath also derived maximum oscillatory shear stresses using the momentum integral technique. The results from these calculations suggest that oscillatory stresses are insensitive to the superposition of a current.

Available field data cover a wide range of sites and wave–current conditions. Two sets of results were reported by Grant et al. (1983) for a site with a water depth of 100 m and a silty bed material; the first set of tests were carried out under spring/summer conditions with an immobile bed, the second set under storm conditions with a large suspended sediment load. Shear stresses deduced from the inertial dissipation method were found to be in good agreement with those from the 4-point log profiles, both sets of results implying an order of magnitude increase in apparent bed roughness felt by the mean flow in the presence of waves. Field tests have also been carried out by Lambrakos et al. (1988) using 5 electromagnetic current meters over an immobile rough bed, and by Slaattelid et al. (1990) using 6 acoustic probes over a mobile sand bed in a vertical profile to determine shear stresses. The Lambrakos data plotted below has been taken from tables presented by Myrhaug and Slaattelid (1989). Huntley and Hazen (1988) carried out tests at 2 sites, while the deployment by Soulsby and Humphery (1990) yielded data for a wide range of current-to-wave ratios at a site with an immobile rough bed. Black et al. (1992) have recently completed field tests which provide information on the spatial variation of wave conditions and shear stresses along a 30 km shore-normal transept over a rippled sandy seabed.

Although the tests described above have been performed under widely differing scales, bed roughnesses, relative wave directions, and methods of calculating shear stress, when time-averaged shear-stresses for all immobile bed tests are plotted together (Fig. 8) they produce a behaviour not dissimilar to that predicted in the previous section by the various models. The general con-

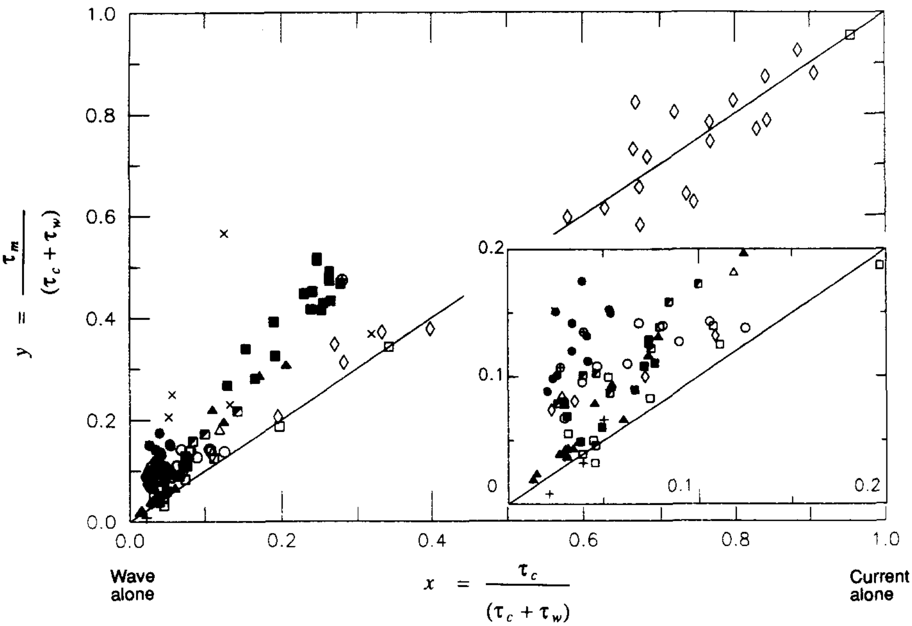

	Authors:	z_0/h	A/z_0	phi (deg)
	Field tests:			
▲	Grant et al. (1983)	2.0 E-5	28-214	30^0, 70^0
⊕	Huntley & Hazen (1988)	2.2,6.0 E-5	45,59	28^0, 9^0
•	Myrhaug & Slaattelid (1989)	7.4 E-6	8100-17000	33^0-48^0
o	Myrhaug & Slaattelid (1989)	1.0 E-4	530-990	46^0-69^0
◊	Soulsby & Humphery (1990)	4.0 E-5	72-564	9^0-70^0
	Laboratory tests:			
Δ	Bakker & van Doorn (1978)	2.3 E-3	100-110	0^0
▨	Kemp & Simons (1982; 1983)	4.0 E-3	14-29	0^0
+	Myrhaug et al. (1987)	1.88 E-2	175-253	0^0
■	Simons et al. (1988)	2.0 E-3	1-21	0^0
□	Simons et al. (1992)	7.1 E-5	600-2390	90^0
×	Sleath (1990)	4.2,26.0 E-4	207-1290	90^0

Fig. 8. Wave-current interaction data: time-averaged bed shear-stresses at different relative current strengths. Inset: blow-up of bottom left corner of main graph.

clusion to be drawn is that non-linear interaction is of most importance under wave-dominated conditions, less so for relatively stronger currents. However, it is worth noting the thinness of data in the current-dominated region. Also, there is very little reliable information on maximum shear stresses under combined wave-current conditions apart from that of Sleath (1990a) and the data generated in the present MAST programme.

Measurements of the oscillatory part of $\tau(t)$ in WCI for $\phi = 90°$ from Sleath (1990a) and Simons et al. (1992) lie close to their corresponding "wave only" values, suggesting that the wave boundary layer is not sensitive to the presence of currents crossing the waves at right angles.

The variation of wave friction factor with relative orbital excursion at the bed (Fig. 9) observed under purely oscillatory flow by Bagnold (1946), Kamphuis (1975), Jonsson and Carlsen (1976), Sleath (1987), Sumer et al. (1987), Simons et al. (1988) and Jensen (1989) shows reasonable agreement with the theory proposed by Myrhaug (1989) and the explicit formula given by Swart (1974)

$$
\begin{aligned}
f_w &= 0.00251\, exp[5.21\,(A/k_s)^{-0.19}] \quad &\text{for } A/k_s > 1.57 \\
&= 0.3 \quad &\text{for } A/k_s \leqslant 1.57
\end{aligned}
\tag{7}
$$

where k_s is the Nikuradse roughness, normally taken to be equivalent to $30z_0$.

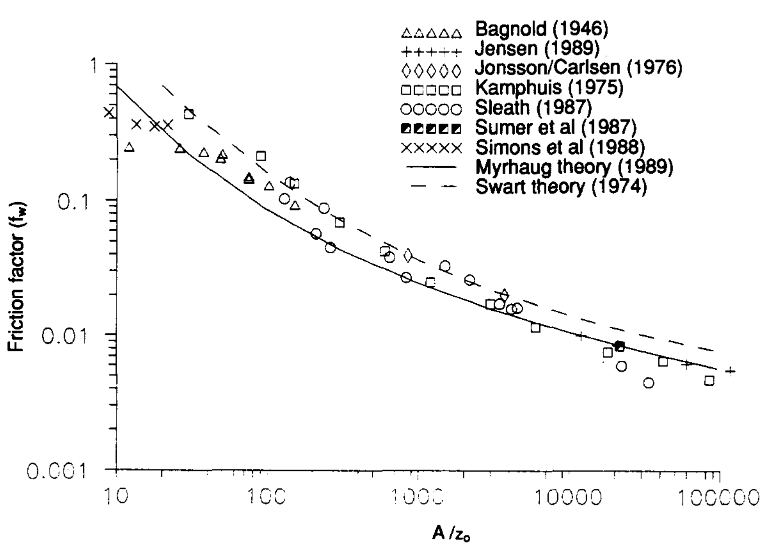

Fig. 9. Variation of wave friction factor f_w with relative bed orbital excursion A/z_0.

Parameterisation

The models of the wave–current boundary layer discussed earlier all require extensive computation to make a prediction of τ_m and τ_{max}. This makes them computationally expensive to use in morphodynamic models of coastal profiles and coastal areas, and simple explicit algebraic methods would be preferable for this purpose. Some of the originators of the models have devised explicit approximations for this purpose (e.g. Yoo, 1989; Tanaka, 1992). However, these are only suited each to a single model. We attempt here to fit one standard formula to all the models, with each model having its own set of fitting coefficients. A second purpose of the parameterisation is to facilitate comparisons between the models and data, although we have not yet advanced that far.

The functions chosen give y and Y as functions of x (all as defined previously) in the forms:

$$y=x[1+bx^p(1-x)^q] \tag{8}$$

$$Y=1+ax^m(1-x)^n \tag{9}$$

where a, m, n, b, p and q are fitting coefficients. Since τ_c, τ_w and hence x are easily calculated from the input parameters, Eqs. (8) and (9) yield y and Y directly, which can in turn be converted to $\tau_m=y(\tau_c+\tau_w)$ and $\tau_{max}=Y(\tau_c+\tau_w)$. It must be emphasized that Eqs. (8) and (9) have no basis in physics, but were merely suggested by the shapes of the curves obtained in the intercomparison exercises (e.g. Fig. 7).

Eqs. (8) and (9) were fitted to the model results for y and Y, respectively, using a nonlinear least-squares technique, for the models considered in the intercomparison exercise. Analytical considerations show that the model of Bijker (1967) is given exactly by Eq. (9) for Y, with $a=2\cos\phi$, $m=n=1/2$. Also the coefficients b, p and q in Eq. (8) for y can be shown to be functions only of ϕ. Likewise it can be shown for O'Connor and Yoo's (1988) extension of Bijker's model, that all the fitting coefficients must be functions of ϕ and (f_w/C_D) only.

This suggested a further parameterisation of the other models. The three models for which the detailed angular dependence was obtained (Fredsøe, 1984; Myrhaug and Slaattelid, 1990; Huynh-Thanh and Temperville, 1991) were therefore fitted to the following functions, by first optimising the coefficients a_1 to a_4, etc, for $\phi=0°$ and $90°$, and then optimising the powers I and J of cos ϕ to give the best overall fit to the model results for all ϕ.

Coefficient a is given by:

$$a=(a_1+a_2|\cos\phi|^I)+(a_3+a_4|\cos\phi|^I)\log_{10}(f_w/C_D) \tag{10}$$

with analogous expressions for m and n.

Coefficient b is given by:

$$b=(b_1+b_2|\cos\phi|^J)+(b_3+b_4|\cos\phi|^J)\log_{10}(f_w/C_D) \tag{11}$$

with analogous expressions for p and q. The resulting coefficients for each model are given in Table 3. A comparison of the fitted expressions with directly calculated model results for the model of Fredsøe (1984) is shown in Fig. 10 for a range of angle ϕ, and is seen to be in reasonably good agreement. In nearly all cases the curves fit the model results to within a relative standard error of 1 to 3%, and a maximum relative error of 5 to 10%. The largest errors in y occur for $0<x<0.05$, and the largest errors in Y occur for ϕ in the region of 75°, where the curves exhibit a slight cubic dependence on x. However, these fitting errors are nonetheless much smaller than the differences between models. We therefore conclude that the use of Eqs. (8) to (11) with the coefficients in Table 3 gives a computationally efficient and acceptably accurate approximation to y and Y for these models.

An improvement on the estimation of y in the region $0<x<0.05$ can be obtained by using the linear interpolation $y=(x/0.05)y(0.05)$, with $y(0.05)$ obtained from Eqs. (8) and (11). However, for these strongly wave-dominated conditions the effect of wave-induced mass-transport velocities will be large, which none of the models is designed to cope with, so that the models themselves will be inaccurate here.

To complete the calculation of τ_m and τ_{max} it is necessary to compute values of C_D and f_w. These should be obtained by interpolation from the values given in Table 4 for each of the three parameterised models if a close simulation of a particular model is required. Alternatively, f_w could be obtained from the

TABLE 3

Fitting coefficients for models of Fredsøe (1984) = F84; Myrhaug and Slaattelid (1990) = MS90; Huynh-Thanh and Temperville (1991) = HT91

	F84	MS90	HT91		F84	MS90	HT91
a_1	−0.06	−0.01	−0.07	b_1	0.29	0.65	0.27
a_2	1.70	1.84	1.87	b_2	0.55	0.29	0.51
a_3	−0.29	−0.58	−0.34	b_3	−0.10	−0.30	−0.10
a_4	0.29	−0.22	−0.12	b_4	−0.14	−0.21	−0.24
m_1	0.67	0.63	0.72	p_1	−0.77	−0.60	−0.75
m_2	−0.29	−0.09	−0.33	p_2	0.10	0.10	0.13
m_3	0.09	0.23	0.08	p_3	0.27	0.27	0.12
m_4	0.42	−0.02	0.34	p_4	0.14	−0.06	0.02
n_1	0.75	0.82	0.78	q_1	0.91	1.19	0.89
n_2	−0.27	−0.30	−0.23	q_2	0.25	−0.68	0.40
n_3	0.11	0.19	0.12	q_3	0.50	0.22	0.50
n_4	−0.02	−0.21	−0.12	q_4	0.45	−0.21	−0.28
I	0.80	0.67	0.82	J	3.0	0.50	2.7

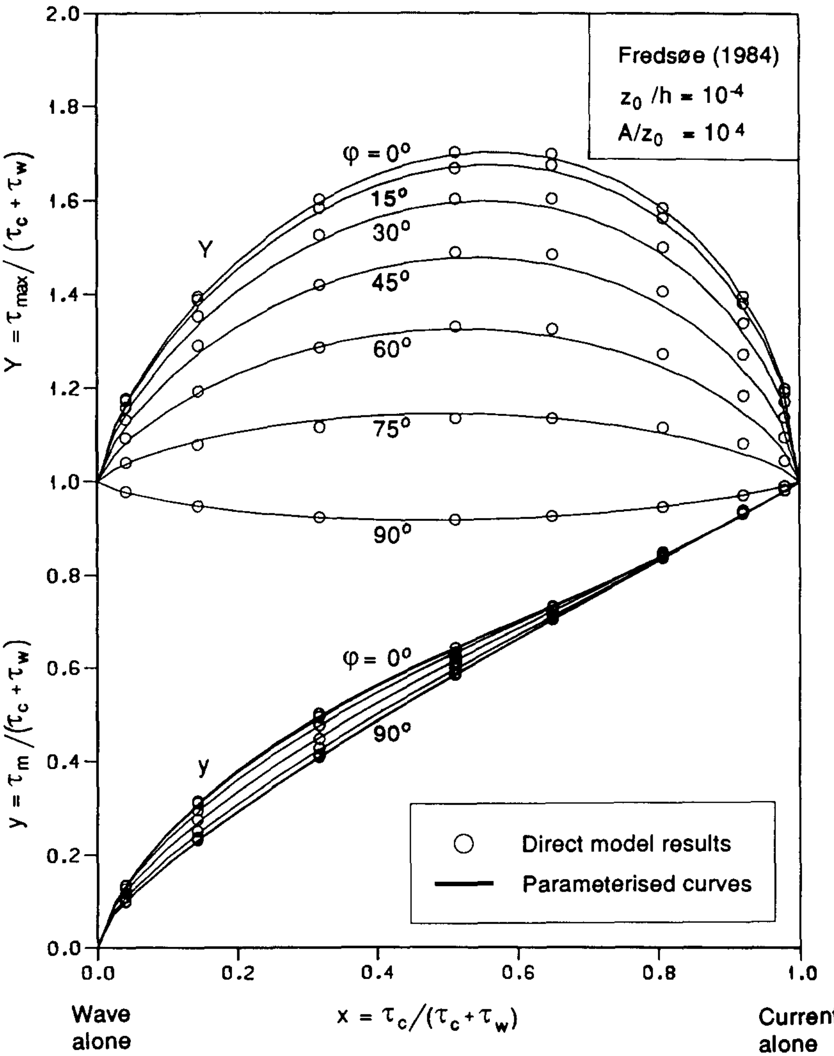

Fig. 10. Comparison of fitted curves with directly computed results from model of Fredsøe (1984), for a range of angles in 15° increments.

Swart formula (Eq. 7) or the method given by Myrhaug (1989), which latter would also allow an extension of the calculation procedure to smooth and transitional flows. Likewise, C_D could be obtained from the logarithmic velocity profile expression:

$$C_D = \left[\frac{0.40}{ln(h/z_0) - 1}\right]^2 \tag{12}$$

TABLE 4

Values of friction factor f_w and drag coefficient C_D from various models (see Table 3 for key). Models F84 and MS90 use the logarithmic profile expression for C_D, Eq. (12)

Values of f_w

	A/z_0			
	10^2	10^3	10^4	10^5
F84	0.0592	0.0221	0.0102	0.0056
MS90	0.0696	0.0233	0.0105	0.0057
HT91	0.0750	0.0272	0.0121	0.0062
Swart (1976)	0.1584	0.0365	0.0141	0.0077

Values of C_D

	z_0/h			
	10^{-2}	10^{-3}	10^{-4}	10^{-5}
F84, MS90	0.01231	0.00458	0.00237	0.00145
HT91	–	0.00482	0.00237	0.00141

A desirable extension of this parameterisation would be to obtain values of the coefficients by fitting Eqs. (8) to (11) to the laboratory and field data. This would combine the physical concepts embodied in the models with the "ground-truth" embodied in the data, to give optimum state-of-the-art estimates of the combined wave–current shear-stresses.

CONCLUSIONS

For the purposes of coastal morphodynamic modelling, we find the following conclusions regarding WCI:

(a) For regular waves without a current, theoretical and semi-empirical approaches are now able to adequately predict near-bottom velocities in the nearshore zone. These methods would need a comprehensive validation against measured data to assess their range of validity, especially in the surf zone. Randomness and directionality of waves require more studies especially with reference to sediment transport.

(b) When a current is added to the waves, for the current profile and wave parameters used in Tables 1 and 2, very good estimates of the wavelengths can be obtained using an appropriate constant current. Good working estimates for the orbital velocities at the bed can also be obtained using the same approximation. These conclusions hold for both linear and nonlinear wave regimes.

(c) A comprehensive model for wave propagation in the presence of a current has shown that the assumption that the bottom boundary layer can be driven by bottom orbital velocities calculated from a separate inviscid model (as in (b) above) is acceptable.

(d) An intercomparison of 8 typical WCI boundary-layer models, with widely differing formulations, showed that the general forms of their predictions of mean (τ_m) and maximum (τ_{max}) bed shear-stress were broadly similar. However, variations between models of up to 30% in τ_{max} and up to a factor of 4 in τ_m were found.

(e) Experimental data for τ_m show some of the broad features predicted by the models, but support for the detailed behaviour is not apparent. Measurements of τ_{max} are only just becoming available, but those made so far appear to indicate that the oscillatory part of the bed shear-stress is not significantly affected by an orthogonal current.

(f) A standard algebraic parameterisation was found to fit all the WCI boundary-layer models with acceptable accuracy, with different models each being represented by a set of fitting coefficients. The prospect of optimising these coefficients against experimental data is anticipated.

ACKNOWLEDGEMENTS

The results reported here represent the work of the whole of the WCI Group of the European Community funded MAST G6M research programme, and not just the authors. The other members include: A.G. Davies, J. Fredsøe, D.A. Huntley, I.G. Jonsson, B.A. O'Connor, P. Sauvaget, B.M. Sumer, A. Temperville, and T. J. Zitman, together with co-workers: A.M. Arnskov, M. Fornerino, S. Huynh-Thanh, C. Liu, M. Mansour-Tehrani, O.H. Slaattelid, M. Thorkilsen, and D. Yoo. Their valuable contributions are greatly appreciated, especially those who did not receive EC funding for their participation. Parts of the work were funded by the Commission of the European Communities Directorate General for Science, Research and Development under Contract No. MAST 0035-C. Other parts were funded by national bodies including: the UK Ministry of Agriculture, Fisheries and Food, the Anders Jahres Foundation for the Advancement of Science, the Netherlands Rijkswaterstaat (Dienst Getijdewateren) as part of the Dutch Coastal Genesis Project, and the French Service Technique Central des Ports Maritime et des Voies Navigables.

R.L.S. wishes to record his indebtedness to Norges Tekniske Høgskole, Trondheim, which he was visiting during the preparation of this paper, and particularly to D. Myrhaug, O.H. Slaattelid, and M. Kjølås. The visit was made possible through a Visiting Senior Scientist Fellowship awarded by the Norwegian Council for Scientific and Industrial Research (NTNF).

NOTATION

a, a_j $(j=1,2,3,4)$	Fitting coefficients
A	$=u_b/\sigma$
b, b_j $(j=1,2,3,4)$	Fitting coefficients
C_D	Current-alone drag coefficient
f_w	Wave-alone friction factor
g	Acceleration due to gravity
h	Water depth (mean-water level to bed)
h_b	Water depth at point of breaking
H	Wave height
H_0	Deep-water wave height
i	$\sqrt{-1}$
I	Fitting coefficient
J	Fitting coefficient
k	Wave-number $(=2\pi/\lambda)$
k_0	Deep-water wave-number
m, m_j $(j=1,2,3,4)$	Fitting coefficients
n, n_j $(j=1,2,3,4)$	Fitting coefficients
p, p_j $(j=1,2,3,4)$	Fitting coefficients
$\tilde{p}$	Complex dynamic pressure
q, q_j $(j=1,2,3,4)$	Fitting coefficients
r_2, r_3	Coefficients
T	Wave period
$\tilde{u}$	Complex 1st order horizontal velocity amplitude of waves
u_b	Amplitude of bottom orbital horizontal velocity of waves
u_{bc}	Bottom orbital horizontal velocity under wave crest
u_{bt}	Bottom orbital horizontal velocity under wave trough
$U(z)$	Current speed at height z
U_{max}	Value of U at water surface
U_{mean}	Depth-averaged current speed
$\tilde{w}$	Complex 1st-order vertical velocity amplitude of waves
x	$=\tau_c/(\tau_c+\tau_w)$
y	$=\tau_m/(\tau_c+\tau_w)$
Y	$=\tau_{max}/(\tau_c+\tau_w)$
z	Vertical coordinate, positive upwards, origin at mean water level
z_0	Bottom roughness length
β	Angle of beach slope
ζ	Complex free-surface elevation
λ	Wavelength
λ_0	Wavelength in deep water

ν	Kinematic viscosity of water
ρ	Density of water
σ	Absolute wave frequency $(=2\pi/T)$
σ_0	Intrinsic (relative) wave frequency
$\tilde{\tau}_{xz}$	Complex horizontal shear-stress
τ_c	Bottom shear-stress due to current alone
τ_m	Mean (cycle-averaged) bottom shear-stress with WCI
τ_{max}	Maximum bottom shear-stress with WCI
τ_w	Amplitude of oscillatory bottom shear-stress due to waves alone
ϕ	Angle between direction of wave travel and current

REFERENCES

Adeyemo, M.D., 1968. Effect of beach slope and shoaling on wave asymmetry. In: Proc. 11th Int. Conf. on Coastal Eng., London. ASCE, pp. 145–172.

Adeyemo, M.D., 1970. Velocity field in the wave breaker zone. In: Proc. 12th Int. Conf. on Coastal Eng., Washington, DC. ASCE, pp. 435–460.

Andrews, D.G. and McIntyre, M.E., 1978a. On wave action and its relatives. J. Fluid Mech., 89: 647–664.

Andrews, D.G. and McIntyre, M.E., 1978b. An exact theory of nonlinear waves on a Lagrangian-mean flow. J. Fluid Mech., 89: 609–646.

Asano, T. and Iwagaki, Y., 1984. Bottom boundary layer in wave–current co-existing systems. In: Proc. 19th Int.Conf. on Coastal Eng., Houston, TX, Ch. 161, pp. 2397–2413.

Asano, T., Nakagawa, M. and Iwagaki, Y., 1986. Changes in current properties due to wave superimposing. In: Proc. 20th Int.Conf. on Coastal Eng., Taipei, Ch. 70, pp. 925–939.

Bagnold, R.A., 1946. Motion of waves in shallow water. Interaction between waves and sand bottoms. Proc. R. Soc., Ser. A, 187: 1–15.

Bakker, W.T. and Van Doorn, T., 1978. Near bottom velocities in waves with a current. In: Proc. 16th Int. Conf. on Coastal Eng., Ch. 82, Hamburg, pp. 1394–1413.

Biesel, F., 1951. Study of wave propagation in water of gradually varying depths. In: Proc. Symposium on Gravity Waves, Circular No. 521, Natl. Bureau of Standards, U.S. Dept. of Commerce, Washington, DC, pp. 243–253.

Bijker, E.W., 1967. Some considerations about scales for coastal models with moveable bed. Publ. 50, Delft Hydraulics Lab., Delft, 142 pp.

Black, K.P., Rosenberg, M., Symonds, G., Simons, R.R., Pattiaratchi, C. and Nielsen, P., 1992. Measurements of the wave, current and sea level dynamics of an exposed coastal site. In: Proc. 6th Int. Conf. on Physics of Estuaries and Coastal Seas (PECS '92), Margaret River, W.A.

Christoffersen, J.B. and Jonsson, I.G., 1985. Bed friction and dissipation in a combined current and wave motion. Ocean Eng., 12(5): 387–423.

Craik, A.D.D., 1982. The drift velocity of water waves. J. Fluid Mech., 116: 187–205.

Dalrymple, R.A., 1973. Water wave models and wave forces with shear currents. Coastal and Ocean Eng. Lab., Univ. of Florida, Tech. Rep. 20.

Davies, A.G., Soulsby, R.L., and King, H.L., 1988. A numerical model of the combined wave and current bottom boundary layer. J. Geophys. Res., 93(C1): 491–508.

Dean, R.G. and Perlin, M., 1986. Intercomparison of near-bottom kinematics by several wave theories and field and laboratory data. Coastal Eng., 9: 399–437.

Deigaard, R., Bro Mikkelsen, M. and Fredsøe, J., 1991. Measurements of the bed shear stress in a surf zone. Inst. Hydrodynamic and Hydraulic Eng., Progress Report 73, pp. 21–30.

Drazin, P.G. and Reid, W.H., 1981. Hydrodynamic Stability. Cambridge University Press, Cambridge, 539 pp.

Dyer, K.R. and Soulsby, R.L., 1988. Sand transport on the continental shelf. Annu. Rev. Fluid Mech., 20: 295–324.

Flick, R.E., Guza, R.T. and Inman, D.L., 1981. Elevation and velocity measurements of laboratory shoaling waves. J. Geophys. Res., 86(C5): 4149–4160.

Fredsøe, J., 1984. Turbulent boundary layer in wave–current motion. J. Hydraul. Eng. ASCE, 110: 1103–1120.

Grant, W.D. and Madsen, O.S., 1979. Combined wave and current interaction with a rough bottom. J. Geophys. Res., 84(C4): 1797–1808.

Grant, W.D. and Madsen, O.S., 1986. The continental-shelf bottom boundary layer. Annu. Rev. Fluid Mech., 18: 265–305.

Grant, W.D., Williams, A.J., Glenn, S.M., Cacchione, D.A. and Drake, D.E., 1983. High frequency bottom stress variability and its prediction in the CODE region. WHOI Technical Report 83-19, Woods Hole Oceanographic Institute, MA.

Hamm, L., Madsen, P.A. and Peregrine, D.H., 1993. Wave transformation in the nearshore zone (review). In: H.J. de Vriend (Editor), Coastal Morphodynamics: Processes and Modelling. Coastal Eng., 21: 5–39.

Hattori, M., 1986. Experimental study on the validity range of various wave theories. In: Proc. 20th Int. Conf. on Coastal Eng., Taipei. ASCE, pp. 232–246.

Hattori, M. and Katsurakawa, T., 1990. Improved calculation of the shoaling wave fields. In: Proc. 22nd Int. Conf. on Coastal Eng., Delft, pp. 396–409.

Huntley, D.A. and Hazen, D.G., 1988. Seabed stresses in combined wave and steady flow conditions on the Nova Scotia continental shelf — field measurements and predictions. J. Phys. Oceanogr., 18(2): 347–362.

Huynh-Thanh, S. and Temperville, A., 1991. A numerical model of the rough turbulent boundary layer in combined wave and current interaction. In: R.L. Soulsby and R. Bettess (Editors), Sand Transport in Rivers, Estuaries and the Sea. Balkema, Rotterdam, pp. 93–100.

Iskandarani, M. and Liu, P.L.-F., 1991a. Mass-transport in two-dimensional water waves. J. Fluid Mech., 231: 395–415.

Iskandarani, M. and Liu, P.L.-F., 1991b. Mass-transport in three-dimensional water waves. J. Fluid Mech., 231: 417–437.

Isobe, M. and Horikawa, K., 1982. Study on water particle velocities of shoaling and breaking waves. Coastal Eng. Jpn., 25: 109–123.

Jensen, B.L., 1989. Experimental investigation of turbulent oscillatory boundary layers. Series Paper 45, Inst. Hydrodym. and Hydr. Eng, Tech. Univ. Denmark, Lyngby.

Jonsson, I.G., 1990. Wave current interactions. In: B. Le Mehauté and D.M. Hanes (Editors), The Sea, Vol. 9A. Wiley-Interscience, New York, pp. 65–120.

Jonsson, I.G. and Carlsen, N.A., 1976. Experimental and theoretical investigations in an oscillatory turbulent boundary layer. J. Hydraul. Res., 14: 45–60.

Kamphuis, J.W., 1975. Friction factors under oscillatory waves. ASCE J. Waterw., Harbors, Coastal Eng. Div., 10(WW2): 135–144.

Kemp, P.H. and Simons, R.R., 1982. The interaction between waves and a turbulent current: waves propagating with the current. J. Fluid Mech., 116: 227–250.

Kemp, P.H. and Simons, R.R., 1983. The interaction between waves and a turbulent current: waves propagating against the current. J. Fluid Mech., 130: 73–89.

Kirby, J.T. and Chen, T.-M., 1989. Surface waves on vertically sheared flows: approximate dispersion relations. J. Geophys. Res., 94: 1013–1027.
Kirkgöz, M.S., 1986. Particle velocity prediction at the transformation point of plunging breakers. Coastal Eng., 10: 139–147.
Klopman, G., 1992. Vertical structure of the flow due to waves and currents. Research on the relevance for sediment transport. Delft Hydraulics, Report H840.30 Part I.
Lambrakos, K.F., Myrhaug, D. and Slaattelid, O.H., 1988. Seabed current boundary layers in wave-plus-current flow conditions. J. Waterw. Port, Coastal Ocean Eng., 114(2): 161–175.
Longuet-Higgins, M.S., 1953. Mass transport in water waves. Philos. Trans. R. Soc. A, 245: 535–581.
Myrhaug, D., 1989. A rational approach to wave friction coefficients for rough, smooth, and transitional turbulent flow. Coastal Eng., 13: 11–21.
Myrhaug, D. and Slaattelid, O.H., 1989. Combined wave and current boundary layer model for fixed rough seabeds. Ocean Eng., 16(2): 119–142.
Myrhaug, D. and Slaattelid, O.H., 1990. A rational approach to wave–current friction coefficients for rough, smooth and transitional turbulent flow. Coastal Eng., 14: 265–293.
Myrhaug, D., Reed, K. and Fyfe, A.J., 1987. Seabed boundary layer studies for pipelines: large scale laboratory experiments. In: Proc. Int. Symp. on Offshore Eng., Rio de Janeiro, pp. 345–359.
Nadaoka, K. and Kondoh, T., 1982. Laboratory measurements of velocity field structure in the surf-zone by LDV. Coastal Eng. Jpn., 25: 125–145.
Nielsen, P., 1984. Explicit solutions to practical wave problems. In: Proc. 19th Int. Conf. on Coastal Eng., Houston, TX. ASCE, pp. 968–982.
O'Connor, B.A. and Yoo, D., 1988. Mean bed friction of combined wave/current flow. Coastal Eng., 12: 1–21.
Peregrine, D.H., 1976. Interaction of water waves and currents. Adv. Appl. Mech., 16: 9–117.
Roelvink, J.A. and Stive, M.J.F., 1989. Bar-generating cross-shore flow mechanisms on a beach. J. Geophys. Res., 94(C4): 4785–4800.
Simons, R.R., Kyriacou, A., Soulsby, R.L. and Davies, A.G., 1988. Predicting the nearbed turbulent flow in waves and currents. In: Proc. IAHR Symposium on Mathematical Modelling of Sediment Transport in the Coastal Zone, Copenhagen, pp. 33–47.
Simons, R.R., Grass, A.J. and Mansour-Tehrani, M., 1992. Experimental study of waves and currents crossing at right angles. In: Proc. 23rd Int. Conf. on Coastal Eng, Venice, pp. 604–617.
Slaattelid, O.H., Myrhaug, D. and Lambrakos, K.F., 1990. North Sea bottom steady boundary layer measurements. J. Waterw. Port Coastal Ocean Eng., 116(5): 614–633.
Sleath, J.F.A., 1987. Turbulent oscillatory flow over rough beds. J. Fluid Mech., 182: 369–409.
Sleath, J.F.A., 1990a. Velocities and bed friction in combined flows. In: Proc. 22nd Int. Conf. on Coastal Eng., Delft, Ch. 35, pp. 450–463.
Sleath, J.F.A., 1990b. Seabed boundary layers. In: B. LeMehauté and D.M. Hanes (Editors), The Sea, Vol. 9. Wiley-Interscience, New York, pp. 693–727.
Sleath, J.F.A., 1991. Velocities and shear-stresses in wave–current flows. J. Geophys. Res., 96(C8): 15237–15244.
Soulsby, R.L., 1990. Tidal-current boundary layers. In: B. LeMehauté and D.M. Hanes (Editors), The Sea, Vol. 9. Wiley-Interscience, New York, pp. 523–566.
Soulsby, R.L. and Humphery, J.D., 1990. Field observations of wave–current interaction at the sea bed. In: A. Tørum and O.T. Gudmestad (Editors), Water Wave Kinematics. Kluwer, Dordrecht, pp. 413–428.
Sumer, B.M., Jensen, B.L. and Fredsøe, J., 1987. Turbulence in oscillatory boundary layers. In: C. Comte-Bellot and J. Mathieu (Editors), Advances in Turbulence. Springer-Verlag, Berlin, pp. 556–567.

Svendsen, I.A. and Buhr-Hansen, J., 1977. On the deformation of periodic long waves over a gently sloping bottom. J. Fluid Mech., 87(3): 433–448.

Swart, D.H., 1974. Offshore sediment transport and equilibrium beach profiles. Delft Hydraulics Lab., Publ. 131.

Swart, D.H. and Crowley, J.B., 1988. Generalized wave theory for a sloping bottom. In: Proc. 21st Int. Conf. on Coastal Eng., Malaga. ASCE, pp. 181–203.

Tanaka, H., 1992. An explicit expression of friction coefficient for wave–current coexistent motion. Coastal Eng. Jpn., 35(1): 83–91.

Tanaka, H., Chian, C.S. and Shuto, N., 1983. Experiments on an oscillatory flow accompanied with a unidirectional motion. Coastal Eng. Jpn., 26: 19–37.

Thomas, G.P., 1981. Wave–current interactions: an experimental and numerical study. Part 1. Linear waves. J. Fluid Mech., 110: 457–474.

Thomas, G.P., 1990. Wave–current interactions: an experimental and numerical study. Part 2. Nonlinear waves. J. Fluid Mech., 216: 505–536.

Trowbridge, J.H. and Madsen, O.S., 1984a. Turbulent wave boundary layers. 1. Model formulation and first-order solution. J. Geophys. Res., 89(C5): 7989–7997.

Trowbridge, J.H. and Madsen, O.S., 1984b. Turbulent wave boundary layers. 2. Second-order theory and mass transport. J. Geophys. Res., 89(C5): 7999–8007.

Trowbridge, J.H., Kanetkar, C.N. and Wu, N.T., 1986. Numerical simulation of turbulent wave boundary layers. In: Proc. 20th Int. Conf. Coastal Eng., Taipei, pp. 1623–1637.

Van Kesteren, W.G.M. and Bakker, W.T., 1984. Near bottom velocities in waves with a current; analytical and numerical computations. In: Proc. 19th Conf. Coastal Eng., Houston, TX. ASCE, pp. 1161–1177.

Visser, 1986. Wave basin experiments on bottom friction due to current and waves. In: Proc. 20th Int. Conf. on Coastal Eng., Taipei, Ch. 61, pp. 807–821.

Yoo, D., 1989. Explicit modelling of bottom friction in combined wave–current flow. Coastal Eng., 13: 325–340.